COOLING THE INTRACLUSTER MEDIUM

P.A. THOMAS

Astronomy Centre, CPES, University of Sussex
Falmer, Brighton, BN1 9QJ, UK

We present N-body, hydrodynamical simulations of galaxy clusters with and without radiative cooling. We find from the non-radiative simulations that most clusters are *not* well-fit by a Navarro, Frenk & White [7] (hereafter NFW) profile, but that nevertheless the NFW model accurately predicts the temperature-mass relations. When measured within a sphere enclosing a fixed overdensity, these all follow the self-similar form, $T \propto M^{2/3}$, however the normalisation is lower than in observed clusters. The temperature-mass relations for properties measured within a fixed physical radius are significantly steeper then this. The effect of adding radiative cooling is to *raise* the temperature and *lower* the X-ray luminosity (except in uncorrected, cooling flow clusters). This tends to bring the simulated L_X-T_X relation into agreement with the observations. We speculate that preheating of group/cluster gas may be unnecessary.

1 Introduction

In this paper, we present results from two sets of simulations of galaxy clusters. We challenge two widely-held beliefs:

- that clusters have a universal density profile (the NFW profile)

- that preheating is required to steepen the L_X-T_X relation.

2 Adiabatic simulations

2.1 The simulations

We have carried out three simulations with 128^3 particles each of gas and dark matter. The cosmological parameters were as follows: density parameter, $\Omega = 1$; cosmological constant, $\Lambda = 0$; power spectrum shape parameter, $\Gamma = 0.21$; and a linearly-extrapolated root-mean-square

Table 1: Run parameters for each of the simulations: box size/h^{-1}Mpc; softening/h^{-1}kpc; dark-matter particle mass/$h^{-1}M_\odot$; minimum resolved cluster mass/$h^{-1}M_\odot$; minimum ratio of the 2-body relaxation time in the core of the clusters to the age of the Universe.

box	soft	$M_{\rm dm}$	$M_{\rm lim}$	$t_{r,\min}/t_0$
50.0	20	1.6×10^{10}	8.22×10^{12}	2.4
112.9	50	1.8×10^{11}	9.47×10^{13}	3.0
153.0	68	4.6×10^{11}	2.37×10^{14}	3.4

dispersion of the density fluctuations on a scale $8\ h^{-1}$ Mpc, $\sigma_8 = 0.60$. The three simulations had different box-sizes, corresponding to different mass-resolutions, as listed in Table 1.

Full details of the simulations and cluster extraction procedure can be found in Thomas et al.[14].

2.2 Density profiles

It is often stated that dark matter halos in CDM cosmologies have a "universal density profile", also known as the NFW profile (Navarro, Frenk & White[7]):

$$\rho = \frac{\rho_0}{x\,(1+x)^2},\tag{1}$$

where $r = ax$ is the radius and ρ_0 and a are free parameters. In order to test this assertion, we introduce a more general profile,

$$\rho = \frac{\rho_0}{x\,(1+x)^s},\tag{2}$$

where s is a constant. We integrate Equation 2 to generate circular velocity curves, then search for the best-fit for each of our clusters. The results are shown in Figure 1. The asymptotic density profile at large radii has a slope of $-(s+1)$. However, this is not always representative of the slope at two virial radii, the outer radius to which we fit the rotation curve. Hence we plot with solid symbols in the Figure only those clusters for which the two differ by less than $0.2s$—this corresponds to a characteristic radius $a < 0.5r_{180}$.

A quick glance at Figure 1 makes the suggestion that $s = 2$ is a universal density profile seem surprising. However, it is hard to measure the density profiles in the outer parts of clusters with any degree of accuracy and the answer that one gets often depends upon the radial extent of the fit. At one virial radius, the slope of the density profile is far from $-(s+1)$ and so the asymptotic slope is poorly constained. In addition, s and a are strongly correlated and it is often possible to get a reasonable fit by forcing $s = 2$ and allowing a to vary. Hence the statement that the profile within one virial radius is 'consistent with and NFW profile' is largely meaningless. It is for this reason that we choose to fit the profile within two virial radii instead.

We define clusters to be consistent with an NFW profile if the asymptotic slope of their density profile lies between -2.8 and -3.2 (i.e. $1.8 < s < 2.2$). Just under a quarter of the clusters meet this criterion.

The best-fit profiles of many clusters plotted with open symbols show a high value of s. However, this does not indicate steep density profiles at large radii because the best-fit core radii rise to compensate. Rather, it indicates that the functional form of the generalised NFW profile is a poor representation of the cluster. As an example consider the cluster shown in Figure 2. This is a smooth cluster: visually it appears spherically-symmetric and it has little substructure. In addition, the best-fitting ellipsoid (see Thomas et al.[13]) is amongst the most spherical of any cluster in our sample with axial ratios of 1.14:1.0:0.94. However, the density profile, even out to 0.8 virial radii, is poorly fit by an NFW profile (dashed line). Also, it shows a sharp change in slope at this radius that cannot be matched by any generalised NFW profile.
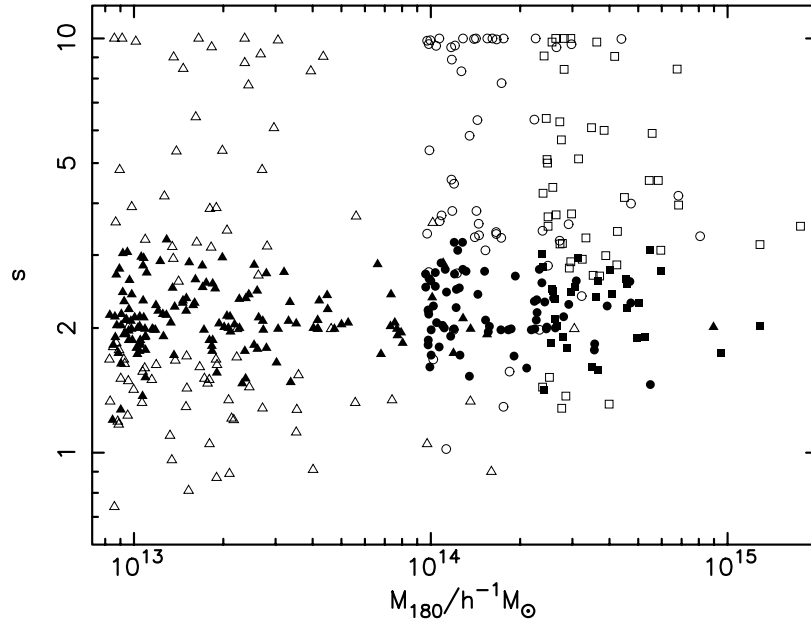
Figure 1: s versus M_{180} for all the clusters. The solid symbols represent clusters for which the slope of the density profile at two virial radii is within 25 per cent of the asymptotic slope at large radii.
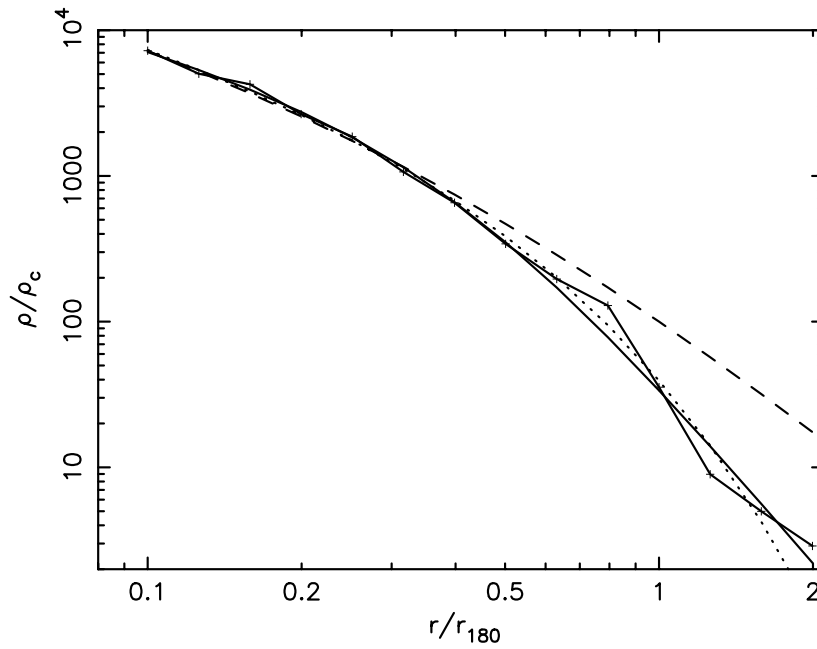

Figure 2: The density profile for one of the clusters. The dashed line shows the best-fit NFW model. The dotted line shows the best-fit generalised NFW model with $s = 10$. The solid line shows a better, alternative model, as described in the text.

The dotted line shows a generalised NFW model with $s = 10.$ and $a = 3.1\,r_{180}$. In order to reproduce the sharp decline in density at the virial radius, s has to be very large, but this then leads to a density profile that is declining far too rapidly in the outer parts of the cluster (and would steepen even more at radii larger than those shown in the Figure). A better representation of the density profile in this case is given by the dotted line which corresponds to the function

$$\rho = \frac{\rho_0}{x\,(1 + x^2)^{s/2}}, \tag{3}$$

where $x = r/a$ as before, and $s = 3.2$, $a = 0.40\,r_{180}$. This value of s is a much better estimate of the asymptotic slope of the density profile at large radii.

It can be seen from Figure 1 that the line $s = 3$ roughly separates the solid from the open symbols in the upper half of the plot. Thus, where the outer slope of the density profile is well-defined, it generally lies between -3 (an NFW profile) and -4 (a Hernquist profile). The open symbols represent clusters, like that shown in Figure 2, that have a sharper break in their density profile than can be fit by a generalised NFW profile: these comprise about 30 per cent of the total cluster sample.

The open symbols that correspond to values of s less than 2 are mostly clusters that show some degree of substructure, for which the density profile is not well-defined. These comprise another 16 percent of the cluster population.

Although the spread in s is large, there is a weak trend for s to increase with mass. To make this more evident, we define an average low-mass and an average high-mass cluster by selecting all relatively smooth clusters, $S < 0.2$, in the mass ranges $M < 1.2 \times 10^{13} h^{-1} \mathrm{M}_\odot$ and $M > 3.0 \times 10^{14} h^{-1} \mathrm{M}_\odot$. The resulting profiles are extremely well-fit by our theoretical model with slopes of $s = 2.0$ and $s = 2.3$, respectively.

It is clear from the above analysis that there is no universal profile for dark matter halos. A substantial proportion of clusters show obvious substructure, and even those that don't exhibit a wide variety of functional forms for the spherically-averaged density profiles of halos.

Despite all this, the concept of a universal density profile is an attractive one. It makes modelling of observed clusters much simpler and it has the advantage that there is only one free parameter—the ratio of the characteristic radius in the NFW formula to the virial radius, $x_{180} = r_{180}/a(s = 2)$.[a] Therefore, we wish to see how well one can approximate cluster properties by assuming that they all follow the NFW profile, in defiance of the above results.

The best-fit values of x_{180} as a function of mass are shown in Figure 3. There is a general trend of decreasing concentration as one moves to higher masses, but once again the scatter is large. The solid line in Figure 3 corresponds to the function

$$x_{180} = 3.7 \left(\frac{M}{10^{15} h^{-1} \mathrm{M}_\odot} \right)^{-0.1}. \tag{4}$$

The 86 per cent of the clusters with modest substructure are spread equally above and below the line. We shall use this relation in the analysis that follows to see how well the simple NFW model predicts the measured scaling relations between temperature and mass.

2.3 X-ray temperature-mass relations within a fixed overdensity

The relationship between X-ray temperature and mass within the virial radius is shown in Figure 4. The dashed line shows the best-fit relation from Evrard, Metzler & Navarro[3] (hereafter

---

[a]NFW define x_{200} to be the 'concentration parameter', presumably using 200 as an approximation for the virial overdensity; in this paper we will use the term to stand for x_{180} instead—there is little difference between the two.
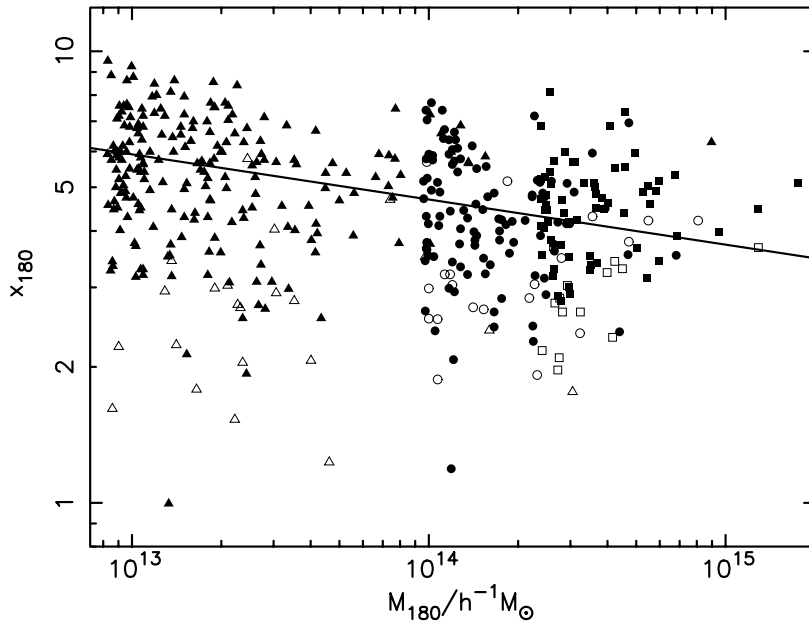
Figure 3: The measured concentration assuming an NFW profile, x_{180}, versus mass within the virial radius, M_{180}, for all the clusters. Clusters with significant substructure are plotted with open symbols; the others with solid symbols.

EMN),

$$k\,T_{X,180} \approx 7.85 \left(\frac{M_{180}}{10^{15}h^{-1}\mathrm{M_\odot}}\right)^{0.67\pm0.02} \mathrm{keV}. \tag{5}$$

They extracted 58 clusters in the temperature range 1–10 keV, from three different sets of cosmological simulations with a variety of cosmological parameters. We have used the information given in their paper to interpolate their results to an overdensity of 180—our results are in good agreement.

The prediction assuming hydrostatic equilibrium of gas in an NFW profile with isotropic velocity dispersions is shown by the solid line on the Figure (for details of the calculation see Thomas et al.[14]). It gives temperatures that are a reasonable fit to the data, but are slightly too low.

The most extensive observational investigation of the T_X-M_{180} relation is by Horner, Mushotzky & Scharf[4] who used many different ways to determine the mass within the virial radius. Their preferred measure, based on X-ray emissivity and temperature profiles, is shown as a dotted line in Figure 4. From this it is clear that either the measured cluster masses are too low, or more likely dissipationless simulations predict X-ray temperatures that are smaller than the observed values. This might be thought to provide evidence for heating of the intracluster medium, but we will argue below that radiative cooling may have the same effect!

In Figure 5, we show a similar plot to Figure 4, but for the X-ray temperature-mass relation within an overdensity contour of 1000. Once again, the isotropic NFW model slightly under-predicts the X-ray temperatures (but agrees with the results of EMN). The best-fit power law is consistent with the self-similar prediction

$$k\,T_{X,1000} \approx 13.0 \left(\frac{M_{1000}}{10^{15}h^{-1}\mathrm{M_\odot}}\right)^{0.67} \mathrm{keV}. \tag{6}$$
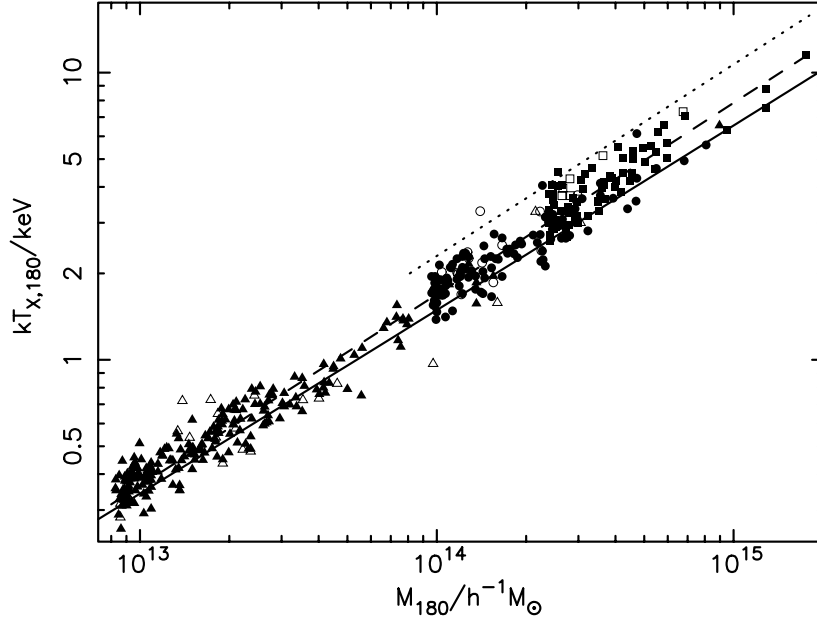
Figure 4: The X-ray temperature versus mass within the virial radius. The dashed line shows the best-fit power law; the dotted line shows the best observational results from Horner, Mushotzky & Scharf and the solid line shows the prediction from the isotropic NFW model.
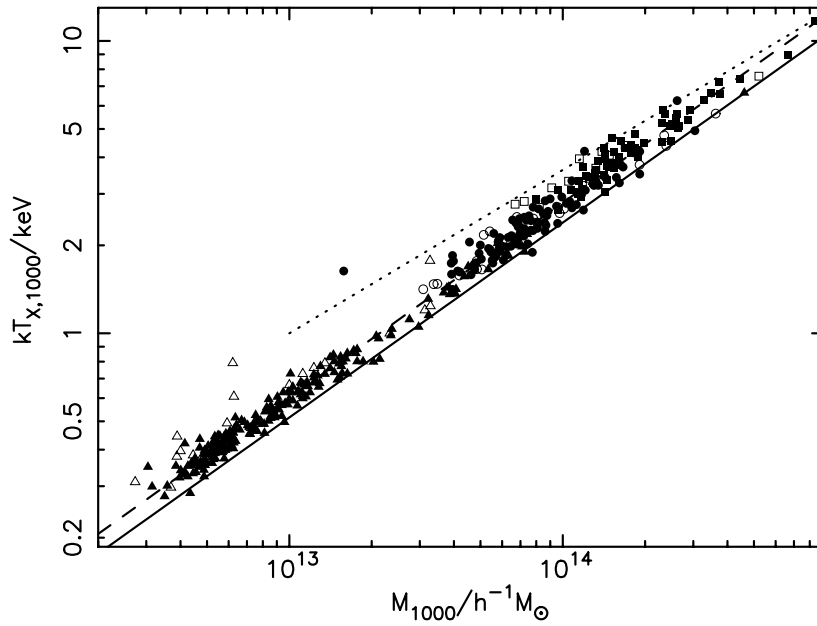

Figure 5: The X-ray temperature versus mass within a spherical shell enclosing an overdensity of 1000. The dashed line shows the best-fit power law, the dotted line shows the observational results from Nevalainen, Markevitch & Forman (2000), and the solid line shows the prediction from the isotropic NFW model.
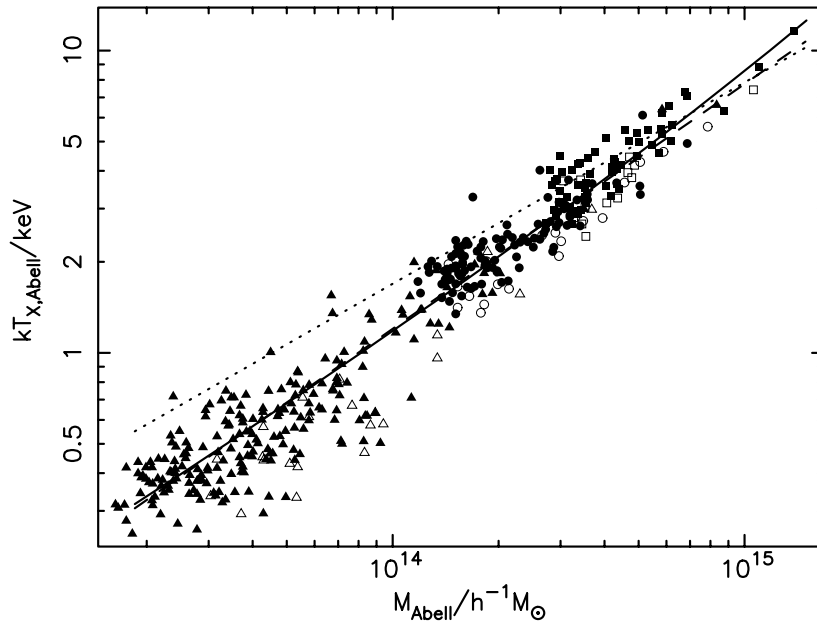
Figure 6: X-ray temperature versus mass, for properties averaged within the Abell radius, for all the clusters. The dashed line shows the best-fit power law. The dotted line is the relation from Equation 5 for properties averaged within the virial radius. The solid line shows a corrected relation based on the NFW model.

The dotted line shows the observational results from Nevalainen, Markevitch & Forman [8]. The observed temperatures are again higher than the predictions from this non-radiative model but in a way that is now mass-dependent—this is consistent with our expectation that the effects of cooling and/or heating would be greater in lower-mass clusters.

2.4   Temperature-mass relations within the Abell radius

On a cautionary note, we should point out that if one measures cluster properties within a fixed radius, rather than a fixed overdensity, then the deviation from the self-similar scaling relations can be quite large. This is shown in Figure 6 where we plot, for properties averaged within the Abell radius, emission-weighted temperature versus mass. The best-fit power law, shown as the dashed line, has a slope of 0.81.

The reason for the steeper slope is that, for low-mass clusters, the Abell radius is greater than the virial radius and so we are averaging properties over a larger volume than before. This has the effect of lowering the X-ray temperature slightly (because the X-ray temperature is heavily weighted by emission from the centre of the cluster this effect is small), but greatly increasing the mass. For high-mass clusters, however, the virial radii are similar to the Abell radii and so there is no change.

3   Simulations with radiative cooling

We next contrast the properties of clusters drawn from simulations with and without radiative cooling. These results are presented at greater length in Pearce et al. [10].

Table 2: The main parameters for each cosmology. The parameters for the cooling and non-cooling runs were identical.

Cosmology	ΛCDM	SCDM
Ω	0.3	1.0
Λ	0.7	0.0
Ω_b	0.03	0.06
σ_8	0.9	0.6
h	0.7	0.5
boxsize (h^{-1}Mpc)	70	50
M_{dm} (h^{-1}M$_\odot$)	1.4×10^{10}	1.6×10^{10}
M_{gas} (h^{-1}M$_\odot$)	1.4×10^9	1.0×10^9
soft (h^{-1}kpc)	10.	10.
Z_{met} (solar)	0.3	0.3

3.1 The simulations

The simulations each follow 2 million gas and 2 million dark matter particles in a box of side 100 Mpc. We have performed simulations in two types of flat cold dark matter cosmology, one standard (SCDM) and one with a cosmological constant (ΛCDM), with parameters as listed in Table 2. In addition to these two simulations which both included the effects of radiative cooling, we repeated the ΛCDM model without cooling. We will concentrate here in the differences between the cooling and non-cooling ΛCDM runs.

The properties of the galaxies in the two simulations with radiative cooling have been described in Pearce et al.[9]. The mass and spatial distribution of the galactic population, and the overall cooled gas fraction are well matched to the observations.

3.2 Intracluster medium profiles

In the next few plots, we show spherically-averaged profiles of the intracluster medium for the 20 largest clusters in the box. The profiles have been centred on the peak of the gas density.

Gas entropy profiles

Gas entropy profiles (and also density and temperature profiles, below) were obtained using only those particles with a temperature exceeding 12 000 K as we wish to exclude cold gas which lies within galaxies or recently tidally disrupted objects. The specific entropy profile is shown in Figure 7. We plot the quantity $(T/\mathrm{K})/(\rho/\bar{\rho})^{2/3}$, where T is the temperature and ρ the density, measured in units of the mean gas density, $\bar{\rho}$.

Let us contrast the results for the ΛCDM runs with and without cooling. Firstly, note that the entropy at the virial radii is very similar in each case—this is because cooling has had little effect at these large radii. Between the virial radius and about 0.2 times the virial radius (less for the largest cluster), the entropy profiles for the cooling run are shallower than in the non-cooling run. This confirms the hypothesis of Thomas & Couchman[12] that cooling is able to *raise* the entropy of the intracluster medium by dragging in high-entropy material from the outer regions of the cluster.

Within about 0.2 virial radii, the entropy profiles again steepen—it is within this "cooling radius" that the cooling time is short enough to allow significant cooling of the gas within the lifetime of the cluster. By the time we get to the innermost bins in the Figure, there seems to
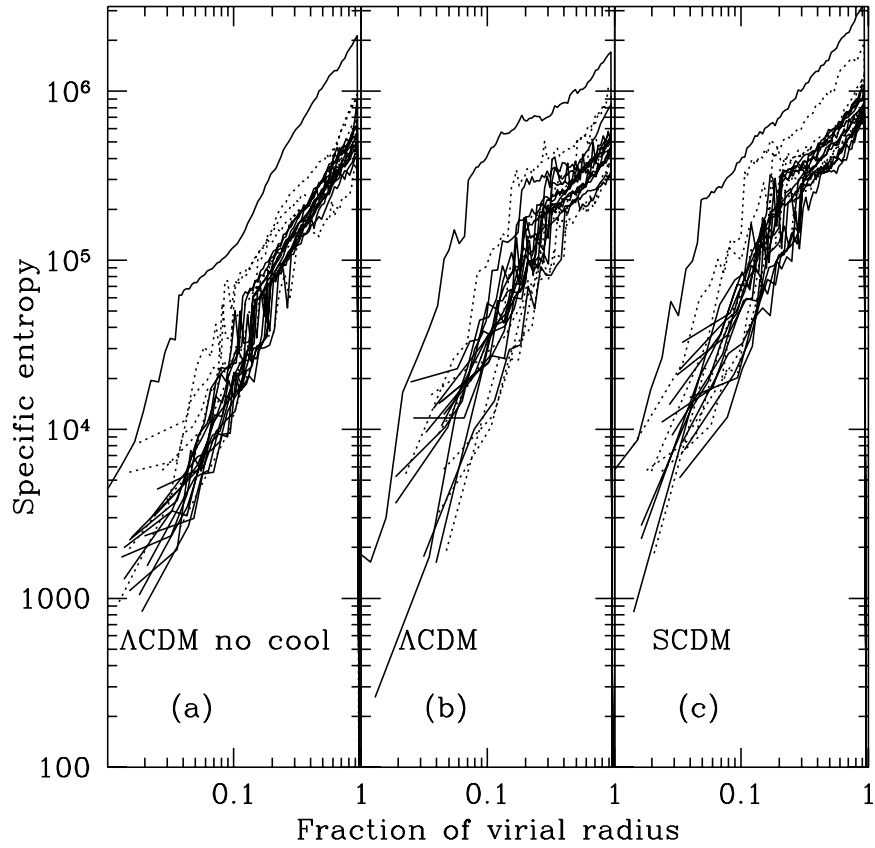
Figure 7: The radial specific entropy profiles of the 20 largest, distinct halos extracted from each of the three simulations. Plotted is the mean value of $T/n^{2/3}$ within successive spherical shells. Each profile has been scaled to the virial radius. Those profiles marked as dotted lines are for clusters that contain significant substructure.
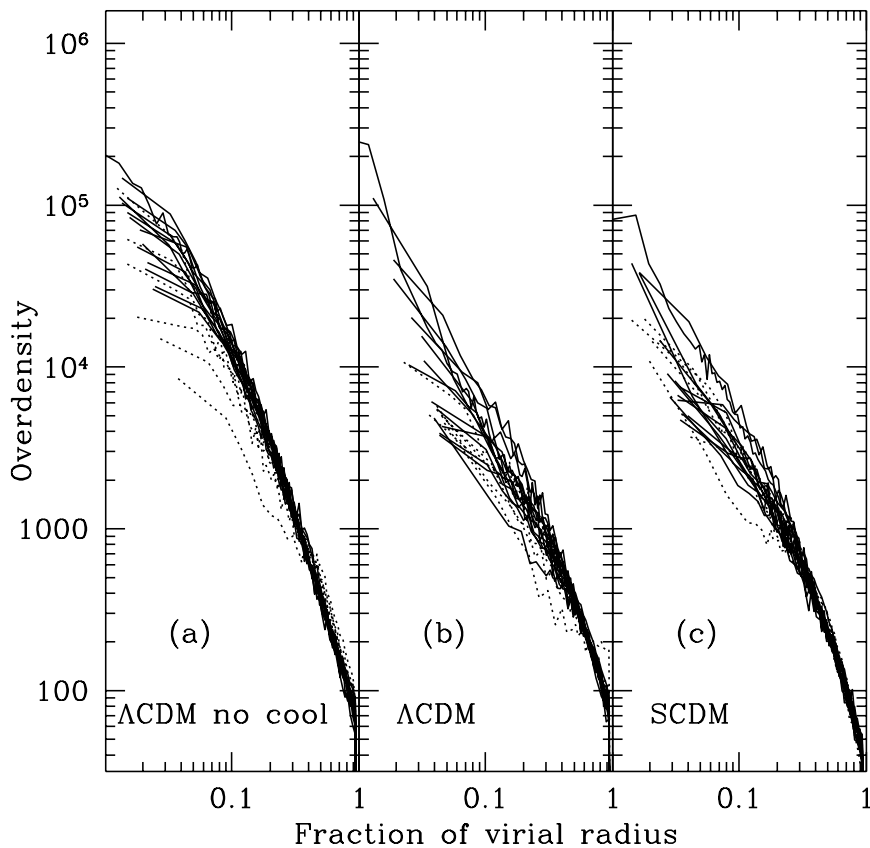
Figure 8: The radial gas density profile of the 20 largest halos found within each simulation. Those halos containing significant substructure are shown as dotted lines. Plotted is the mean gas density within successive spherical shells. All the halos are scaled to the virial radius and gas overdensity relative to the baryonic cosmic mean.

be a spread in the entropy of the clusters in the cooling run, with some having higher entropy and some lower entropy than the corresponding clusters in the non-cooling run.

Gas density profiles

The radial gas density profiles are displayed in Figure 8. The effect of cooling is to *lower* the gas density at all radii within the virial radius. The suppression is greatest, a factor of three, at about 0.1 times the virial radius, roughly corresponding to the kink in the entropy profiles seen in Figure 7. Although the density gradients are shallower, they do not roll over into constant-density inner core regions. In fact, for the larger clusters, the density continues to rise further into the centre of the cluster than before, so that the central density is close to that in the non-cooling case.

The profile of the largest object in both gas and dark matter for each of the runs is shown in Figure 9. The arrow indicates a radius of $100\,h^{-1}$kpc. Without cooling, the gas density is shallower than that of the dark matter within 0.1 times the virial radius, but this inner, resolved slope of the density profile is still $\rho \propto r^{-1}$ with no sign of a constant-density core. As the temperature is approximately constant within this region (see Figure 10), the X-ray luminosity is convergent and dominated by emission from around $200\,h^{-1}$kpc (0.1 times the virial radius).

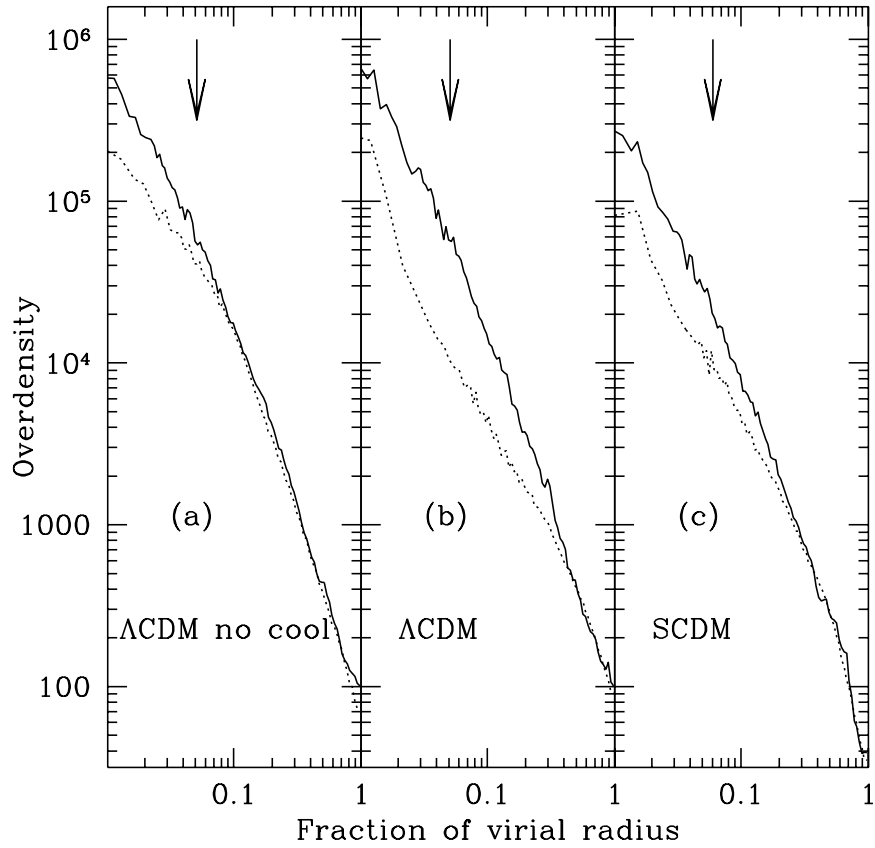With cooling, the largest cluster exhibits a central density spike due to the presence of a

Figure 9: The radial dark matter (solid line) and gas (dotted line) density profile within the virial radius of the largest dark matter halo extracted from each simulation. Each curve is scaled to the virial radius of the halo and overdensity of the appropriate phase relative to the mean cosmic density of that phase. In all three runs there is less gas within the virial radius than dark matter, relative to the cosmic mean of each species. No constant density core is found in the cooling runs. The arrow indicates a scale of $100h^{-1}$kpc.

massive central galaxy. This hot gas has a very steep radial density profile, $\rho \propto r^{-3}$, and would be classified observationally as a cooling flow of $60h^{-2}\mathrm{M}_\odot/\mathrm{yr}$ onto the central cluster galaxy. Between radii of about $40\,h^{-1}\mathrm{kpc}$ and $1\,h^{-1}\mathrm{Mpc}$, the density profile is a power law, $\rho \propto r^{-1.4}$, steepening at larger radii. Thus the X-ray luminosity (excluding the cooling flow) comes from a much more extended region than in the non-cooling case.

In conclusion, the gas density has been reduced by the influx of high-entropy material, as expected. However, this has not given rise to constant-density inner cores. In fact, if anything, the density profiles now continue as a power-law closer into the centre of the clusters.

3.3 Radial temperature profiles

Radial temperature profiles are shown in Figure 10. They rise inwards from the virial radius by about a factor of two, peaking at about 0.1 times the virial radius and then declining again, very gradually, in the cluster centre. Cooling makes little difference to the temperature profiles, except that corresponding clusters in the ΛCDM runs reach a *higher* peak temperature when cooling is implemented, due to the inflow of higher entropy gas. The temperatures are very similar at the virial radius, but are about 1.5 times higher at their peak than before. Two clusters show a precipitous decline in temperature in the cluster centre, one of these being the largest cluster—this is evidence for a cooling flow.

3.4 X-ray luminosity profiles

The total X-ray luminosity within the virial radius of each of the clusters is much reduced for clusters in the simulation with cooling compared to those those from the corresponding non-cooling run. This contradicts the previous results of Katz & White [5], Suginohara & Ostriker [11] and Lewis et al. [6] who all found the X-ray luminosity increased if cooling was turned on. The reason for the discrepancy is that we have decoupled the hot and cold gas, thus greatly suppressing the cooling of the inflowing, high-entropy gas in our simulations compared to previous ones. This causes a large reduction in the mass of the brightest cluster galaxy compared to those produced by previous work. Our galaxies have reasonable luminosities, mass-to-light ratios and number counts for a volume of this size.

Note that estimates of X-ray luminosity from the non-cooling run are not really meaningful. A radiation rate of this magnitude can only be sustained for a short time before depleting the intracluster medium of gas, as in the cooling runs. The X-ray luminosity in the cooling runs is more physically self-consistent and numerically robust. The X-ray luminosity within the cooling radius is approximately equal to the enthalpy of the gas divided by the age of the cluster.

We plot these bolometric luminosities as a function of radius for each of our clusters in Figure 11. The relative contribution to the total X-ray emission from different radii is very different for the cooling and non-cooling simulations. Without cooling all the relaxed clusters show very similar emission profiles, with only a small contribution to the total emission coming from the very centre. Once radiative cooling is turned on the radial emission profiles span a much broader range. For two of the clusters, a central cooling flow type emission is clearly visible — contributing 50 percent and 80 percent of the total X-ray flux. For each of the other clusters, the radius enclosing half of the total emission is much larger than that for the simulation without cooling.

3.5 L_X–T_X relation

There has been much debate in the literature centering on the X-ray cluster L_X versus T_X correlation. The emission weighted mean temperature is plotted against the bolometric luminosity
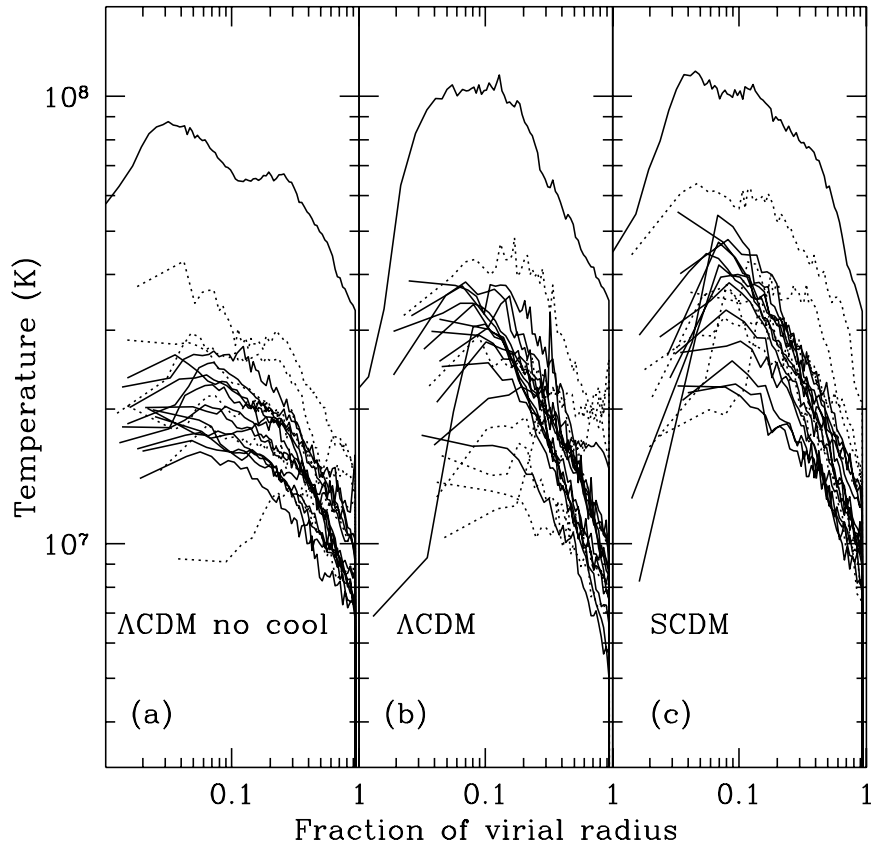
Figure 10: The radial gas temperature profile found within each of the 20 halos extracted from each cosmology. Clusters with significant substructure are marked as dotted lines. All the halos are scaled to the virial radius and temperatures (calculated as the mass-weighted mean temperature of the gas within successive spherical shells) are in Kelvin. With cooling the cluster temperature reaches a slightly higher maximum at a larger fraction of the virial radius whereas the temperature at the virial radius is very similar.
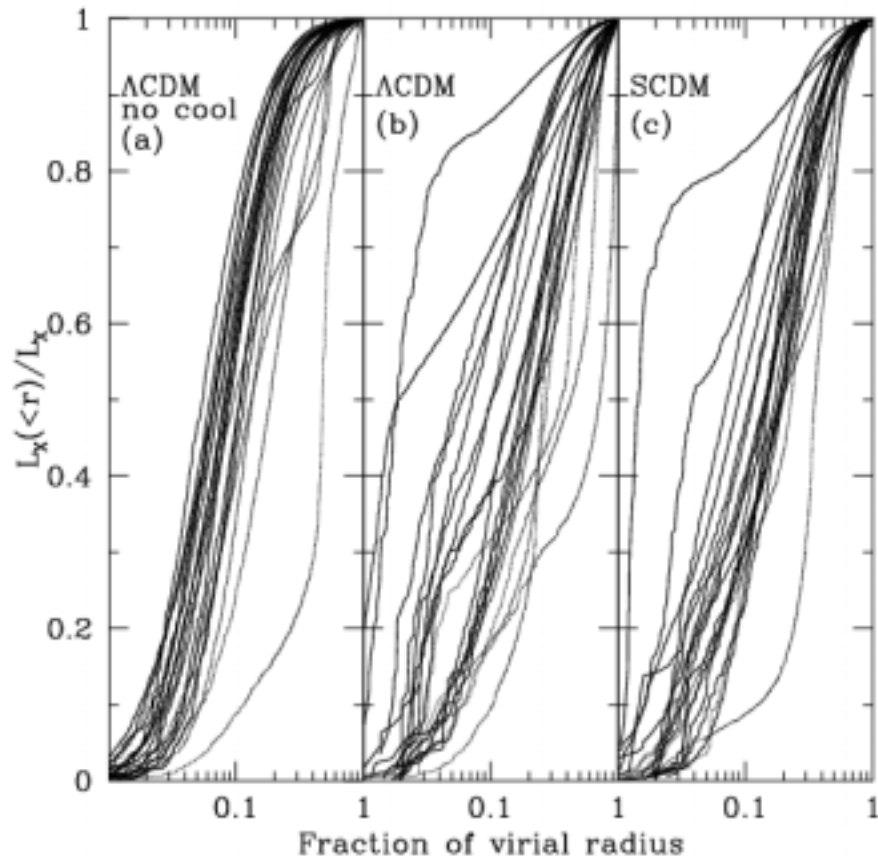
Figure 11: The fraction of the total bolometric luminosity that is emitted from within the specified radius for each of the clusters. Clusters with significant substructure are shown as dotted lines.
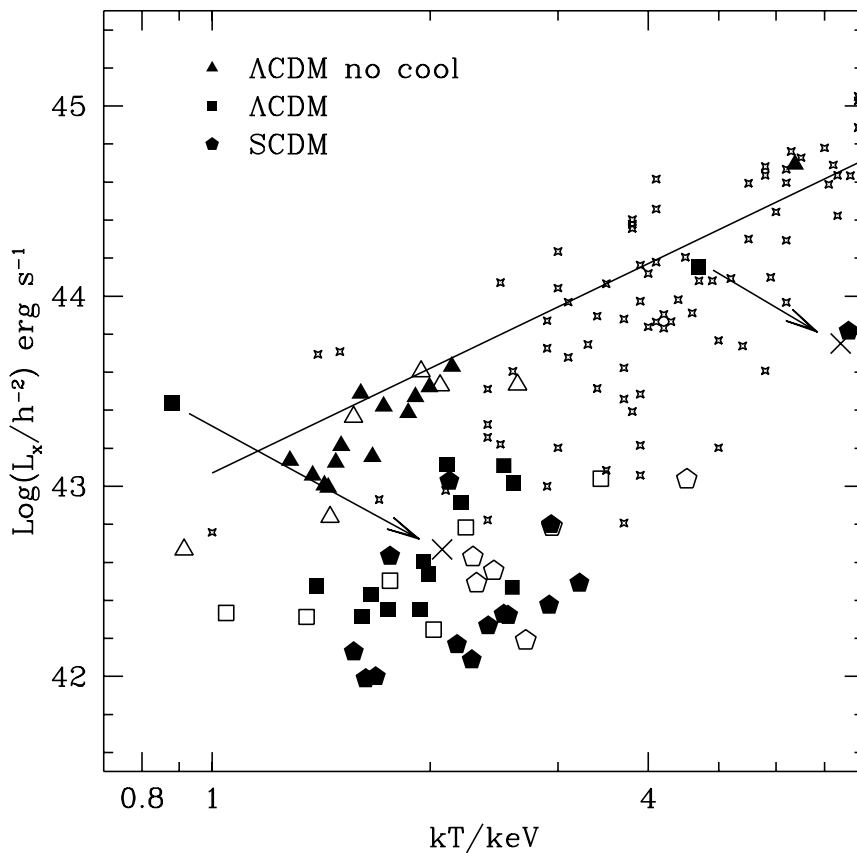
Figure 12: The luminosity-temperature relation for all the clusters. Open symbols refer to those clusters with significant substructure, filled to those without. The small symbols are the observation data from David, Jones & Forman. The majority of our clusters are small because the simulation volume is only 100Mpc on a side but span a reasonable range. The values plotted are the emission weighted mean temperature converted to keV and the bolometric luminosity within the virial radius. The regression line is that of Eke, Navarro & Frenk, Figure 16. and represents a fit to the X-ray luminosity of their ΛCDM clusters. The crosses show where the two ΛCDM clusters indicated would appear on the diagram if their central cooling flow emission was removed from both the bolometric X-ray and emission weighted temperature calculations.

within the virial radius for all our clusters in Figure 12. The filled symbols represent the relaxed clusters and the open symbols denote those clusters that show significant substructure.

The effect of cooling is, in general, to slightly raise the temperature but to greatly reduce the X-ray luminosity. Exceptions are the cooling flow clusters where the large amount of emission from gas cooling onto the central galaxy gives rise to a lower temperature than in the non-cooling case. There are two of these, easily visible on the plot, in the ΛCDM run; we have plotted their new locations, when the central cooling flow is omitted, using crosses linked to the old location via arrows. In both cases less than 2 percent of the hot, X-ray emitting particles were excised to make this calculation.

All 3 sets of clusters display a positive correlation between L_X and T_X, although there are insufficient numbers to tie the trend down very tightly. It is clear from the comments in the preceding paragraph that the nature of the correlation depends critically upon whether one removes the cooling flow emission or not. We believe that a clearer picture arises if this is done.

The regression line in Figure 12 is from Eke, Navarro & Frenk[2] and corresponds to $L_X \propto T_X^2$. Our non-cooling clusters fit reasonably well with this relation. The cooling clusters lie below

this line. Given that we expect cooling to be less important in the most massive clusters (the absolute value of the cooling time and the ratio of the cooling time to the dynamical time both increase with cluster mass), then we would expect the clusters with radiative cooling to lie closer to the regression line at higher T_X. Thus the effect of cooling should be to steepen the L_X–T_X relation. We hope to test this with more simulations of higher mass clusters.

4 Conclusions

- Clusters do *not* have a universal density profile, although a model of gas in hydrostatic equilibrium within an isotropic NFW profile for the dark matter does reproduce the measured temperature-mass relation reasonably well.

- We speculate that preheating may not be required to explain the steep L_X–T_X relation in galaxy groups and clusters as radiative cooling has a similar effect.

References

1. David L. P., Jones C., Forman W., *Astrop. J.* **445**, 578 (1995)
2. Eke V. R., Navarro J. F., Frenk C. S., *Astrop. J.* **503**, 569 (1998)
3. Evrard A. E., Metzler C. A., Navarro J. F., *Astrop. J.* **469**, 494 (1996)
4. Horner D. J., Mushotzky R. F., Scharf C. A., *Astrop. J.* **520**, 78 (1999)
5. Katz N., White S. D. M., *Astrop. J.* **412**, 455 (1993)
6. Lewis G. F., Babul A., Katz N., Quinn T., Hernquist, L., Weinberg, D. H., *Astrop. J.* **536**, 623 (2000)
7. Navarro J. F., Frenk C. S., White S. D. M., *Astrop. J.* **490**, 493 (1997)
8. Nevalainen J., Markevitch M., Forman W., *Astrop. J.* **532**, 694 (2000)
9. Pearce F. R., et al., *Astrop. J.* **521**, L99 (1999)
10. Pearce F. R., Thomas P. A., Couchman H. M. P., Edge A. C., *Mon. Not. R. astr. Soc.* in press, astro-ph/9912013, (2000)
11. Suginohara T., Ostriker J. P., *Astrop. J.* **507**, 16 (1998)
12. Thomas P. A., Couchman H. M. P., *Mon. Not. R. astr. Soc.* **257**, 11 (1992)
13. Thomas P. A. et al. (the Virgo Consortium), *Mon. Not. R. astr. Soc.* **296**, 1061 (1998)
14. Thomas P. A., Muanwong O., Pearce F. R., Couchman H. M. P., Edge A. C., Jenkins A. R., Onuora L., *Mon. Not. R. astr. Soc.* submitted, astro-ph/0007348, (2000)